New Method for Isotopic Ratio Measurements of Atmospheric Carbon Dioxide Using a 4.3 μm Pulsed Quantum Cascade Laser

David D. Nelson[1], J. Barry McManus[1], Scott C. Herndon[1], Mark S. Zahniser[1], Bela Tuzson[2] and Lukas Emmenegger[2]

[1]***Aerodyne Research, Inc., 45 Manning Road, Billerica, MA 01821-3976, USA***
[2]***EMPA, Swiss Federal Laboratories for Materials Testing and Research, Laboratory for Air Pollution and Environmental Technology, Uberlandstr. 129, 8600 Dübendorf, Switzerland***

fax: +1 978 663 4918 (Aerodyne Research); +41 44 821 6244 (EMPA)
email: ddn@aerodyne.com, mcmanus@aerodyne.com, herndon@aerodyne.com, mz@aerodyne.com, bela.tuzson@empa.ch, lukas.emmenegger@empa.ch

Abstract

We present a new approach to the measurement of stable isotopic ratios of carbon dioxide using a near room temperature pulsed quantum cascade laser and a spectral ratio method based upon dual multiple pass absorption cells. The spectral ratio method improves precision and accuracy by reducing sensitivity to variations in the laser tuning rate, power and line width. The laser is scanned across three spectral lines (near 2310 cm^{-1}) quantifying three CO_2 isotopologues: $^{12}C^{16}O_2$, $^{13}C^{16}O_2$ and $^{12}C^{16}O^{18}O$. Isotopic ratios are determined simultaneously with a precision of 0.2 δ for each ratio with a one second measurement. Signal averaging for 400 seconds improves the precision to better than 0.03 δ for both isotopic ratios (^{13}R and ^{18}R). Long term accuracy of 0.2 to 0.3 δ is demonstrated with replicate measurements of the same sample over a one month period. The fast time response of this instrument is suitable for eddy flux measurements.

PACS classification codes: 07.57.Ty; 42.62.Fi; 92.70.Cp; 91.67.Rx

1. Introduction

Real time methods to monitor the stable isotopic ratios of carbon dioxide are needed to improve our understanding of the sources and sinks of this centrally important greenhouse gas [1-4]. Numerous isotopologues of CO_2 may be studied, which tell researchers different things, according to how different sources (and sinks) are enriched or depleted, and by how the physical and biological interactions in the environment alter the isotopic abundances [5-10]. Changes in relative abundances of different isotopologues on the order of 10^{-4} (or 0.1 ‰) may have significance in analysis of sources and sinks. Real-time continuous in-situ measurement of isotopic ratios, performed with ambient CO_2 concentrations, would offer numerous advantages to atmospheric and environmental research. Isotopic ratio fluctuations may be usefully correlated with a variety of other measurements (e.g. wind, temperature, moisture), and with sufficient speed and precision of isotopic measurement isotopic fluxes may be derived [11]. The standard method of measuring isotopic abundances is with mass spectrometry, a method which provides high precision (<0.1 ‰) , but which is unsuited to real-time continuous analysis or field deployment [12-14].

This paper describes recent efforts to address the challenge of real-time high precision measurement of isotopic ratios of carbon dioxide using infrared absorption spectroscopy with a pulsed, room-temperature quantum cascade (QC) laser. Laser absorption spectroscopy previously has been used for real-time measurement of isotopic ratios of CO_2 with good results [15-22]. FTIR absorption spectroscopy has also been applied to this problem [23]. The best results obtained to date have been with cryogenically cooled lead-salt diode lasers [16]. Lead-salt TDL's typically operate continuously, with narrow linewidths, but with several problems for field settings, including unstable operation characteristics, low power, and the need for cryogenic temperatures. QC lasers operating in the pulsed mode have several advantages that enable their deployment in the field as optical sources: absence of cryogenic fluids; stable single mode spectral output; and high power.

Despite the advantages of pulsed QCL's, there are numerous problems to be overcome in performing precision measurements with pulsed sources. Pulsed laser operation introduces additional noise, via pulse to pulse output energy variation and instability of the laser frequency. Pulsed laser operation also leads to frequency broadened output, as the laser tends to chirp during each pulse as the laser warms transiently. However, pulsed operation has the advantage of suppression of optical interference fringes compared to continuous wave lasers [24, 25].

Recent advances in instrument design and signal processing allows us to significantly reduce some of the problems associated with precision spectroscopic measurements with pulsed lasers. The instrument design described here represents significant progress in meeting our goals of measuring the stable isotopologues of atmospheric CO_2 with high precision (<0.1 ‰), accuracy (0.2 ‰ in replicate measurements) and speed (0.2 ‰ in 1 second), and with ambient concentration levels (no pre-concentration). The instrument package is relatively small and is suitable for field deployment. In the selected spectral region [21], one can measure three isotopologues simultaneously, [266], [366], [286] (using HITRAN notation where, e.g. [366] = [$^{13}C^{16}O_2$] [26]). Thus, this instrument reports two delta values ($^{13}\delta$ and $^{18}\delta$) for sampled air at the same time.

2. Experimental

2.1 General spectral measurement approach

Our general approach to atmospheric trace gas measurements using tunable infrared laser differential absorption spectroscopy with pulsed QC lasers (QC-TILDAS) has been described previously [27, 28]. We use rapid laser frequency sweeps and long path, reduced pressure, multiple pass absorption cells [29, 30] to obtain absorption spectra with high signal to noise ratio. We perform nonlinear least squares fits to the acquired spectra using the fundamental spectroscopic constants to determine the mixing ratios of the trace gas species. We use an optical system that consists mostly of reflective optics in order to minimize optical interference fringes. In this work, the laser is cooled

to -28 C with a Peltier cooler. The infrared detectors are cooled with liquid nitrogen. We have used InSb photodiodes and HgCdTe photodiodes with similar results.

We frequently use a "pulse normalization" technique to account for laser amplitude noise [27, 28]. To implement pulse normalization, a beam splitter generates an optical path that does not pass through the sample multipass cell. Simultaneous detection of this normalization beam produces a normalization spectrum. Each sample spectrum is divided by the corresponding normalization spectrum before spectral analysis. This procedure produces a normalized sample spectrum with a much flatter baseline and with considerably reduced laser amplitude noise.

We have selected the 2310 cm^{-1} spectral region to measure CO_2 isotopic ratios, where the line set {2310.00, 2310.21, 2310.35 cm^{-1}} corresponds to isotopologues {[266], [286], [366]}. A typical spectrum, acquired with one second averaging time, is shown in Figure 1. The optical depth of each isotopic variant is similar, ~ 10 – 15%. This implies that the line strength, S, for the major isotope is much weaker than those for the minor isotopic variants. The transition for the major isotope involves a lower state with temperature dependent filling, which produces a strong temperature dependence of linestrength, and which requires careful control and measurement of the temperature. For the lines that we have selected (^{13}S / ^{12}S) varies by 13 ‰/K and (^{18}S / ^{12}S) varies by 19 ‰/K.

The spectrum in Figure 1 was acquired under typical operating conditions of: sample pressure of 60 Torr, sample temperature of 305 K and sample optical path length of 7.0 meters. The laser sweep rate was 4.8 kHz and the effective laser line width was 0.016 cm^{-1} (HWHM). We estimate that the average power reaching the sample detector was approximately 8 μW. This implies that the peak power was about 800 μW, with the laser pulsing with 1% duty cycle (1 MHz repetition rate, 10 ns pulse duration).

2.2 Spectral ratio method

In order to obtain measurement precision of ~ 0.1‰ we have extended our normalization approach to pulsed laser trace gas measurements, with a new "spectral ratio" method. This method implemented by installing a second multiple pass cell and by directing the normalization beam through this reference cell. In this dual-cell arrangement, ambient air flows through the sample cell and a (low cost) working-standard gas flows through the reference cell. The reference gas can be any pressurized CO_2 and (dry) air mixture, preferably with concentration and isotopic composition close to ambient.

Spectral analysis is applied to the ratio of the sample and reference spectra. The reference gas mixing ratio is chosen to be similar to the atmospheric mixing ratio. In this way the spectral ratio has much smaller absorbance than either the sample or reference spectra. In addition, to reducing laser amplitude noise and baseline curvature, this approach improves the accuracy of the isotopic ratio measurement since the sample mixing ratios are continually referenced to the stable isotopic ratios in the reference gas. This significantly reduces potential errors in the derived isotopic ratios due to

uncertainties in the sample temperature, laser tuning rate, laser line width and spectral fitting procedures. A normalized sample spectrum is shown in Figure 2, where in this example there is less absorbance in the sample cell than in the reference cell. The spectral transmission appears to be negative, and with a peak absorbance approximately 100 times smaller than the absorbance in the un-normalized spectrum (Figure 1). While concentration analysis proceeds using the divided spectra, we use un-divided spectra (with much greater depth) to monitor and control the laser spectral position.

The usual approach to determining mixing ratio using direct absorption spectroscopy relies on the Beer-Lambert law and the ideal gas law. Using these two principles, it is easy to show that the sample mixing ratio is given by:

$$M_s = k/(\sigma(T)*L) * A * (T/P) \quad , \quad (1)$$

where M_s is the mixing ratio, k is Boltzmann's constant, σ is the temperature dependent integrated cross section for the spectral line, L is the optical path length, A is the measured integrated absorbance and T and P are the sample temperature and pressure. Expression 1 is modified when using the spectral ratio method, so that the mixing ratio is given by the sum of two terms:

$$M_s = k/(\sigma(T)*L) * A_N * (T/P) + M_r * (P_r/P) * (T/T_r) * (\sigma(T_r)/(\sigma(T)) \quad , \quad (2)$$

where M_r is the reference gas mixing ratio, A_N is the integrated absorbance of the normalized spectrum and T_r and P_r are the reference gas temperature and pressure. The second term is typically larger when the spectral ratio method is used, since the sample mixing ratio is approximately equal to the reference mixing ratio and little normalized absorbance is observed. The benefits of this method are most obvious in the case where the sample spectrum is identical to the reference spectrum. In this case $A_N = 0$ and the first term vanishes. If the sample temperature and pressure are identical to those in the reference cell, then the sample mixing ratio is the same as the reference mixing ratio and knowledge of the laser parameters and accuracy in the fitting procedures are nearly irrelevant. Since we compute mixing ratios based on nearly cancelled spectra, proportional noise in the measurement of the integrated absorbances is much less important. This relaxes the requirements on the stability of the laser tuning rate, the laser line width and the spectral fitting routines. Since the line strength temperature dependence enters as a ratio, the derived isotopic ratio is sensitive to the temperature difference between the two cells rather than their absolute temperatures.

Two techniques are employed to deal with the temperature sensitivity of the linestrengths. Combining accurately measured pressure and temperature differences with Equation (2) gives a prescription for deriving the sample mixing ratio when the two cells are at different pressures or temperatures. At the same time, we carefully control the cell pressures and temperatures to reduce their differences. By maintaining small differences between the cells we also minimize second order effects, such as changes in absorption line shape with pressure and temperature.

2.3 Optical layout for spectral ratio method

The Quantum Cascade Laser Carbon Isotope Spectrometer (QCLCIS) optical module is designed to evenly split the light from the QC laser, direct the two beams through matched absorption cells (sample and reference) and then focus the beams onto separate, but very similar detectors. The optical paths outside the cells are of matched lengths, in order to reduce the effects of background CO_2 absorption. The optical module also is purged with CO_2 free air during measurements. The optics are mounted on a heated, temperature controlled baseplate (with cover), measuring 0.43 x 0.64 m. The cells are positioned adjacent to each other and housed in a separate aluminum enclosure, within the heated optical table enclosure, for further temperature stabilization. The design is illustrated in Figure 3, which was produced in "TracePro", a program for solid modeling and ray tracing.

The optical train begins with a quantum cascade laser, mounted in a sealed temperature controlled and water cooled housing, with pulser electronic board attached. A 15x reflecting objective collects and refocuses the light emitted from the laser. The objective is mounted on a three-axis translation stage which allows fine adjustment of the focus. The initial focus is adjusted to be at a reference pinhole, which serves as the anchor for the optical system. The pinhole is used during initial alignment, and then is folded out of the beam for use. A visible "trace" laser is mounted on a separate assembly, which kinematically drops into the beam path to provide a means of visual alignment of the optical system. In addition, an eyepiece can drop into the pinhole location, so that one may look back at the laser with a magnification of 150. We then adjust the 15x objective position to place the laser image in the center of the pinhole, and thus ease the task of initially finding the infrared light signal.

Beyond the initial focus, a pair of curved mirrors, one concave and the other convex, are used to produce a narrow high F-number beam that is well matched to the optical multi-pass cells. A wedged zinc selenide beamsplitter produces two beams of nearly equal power. The beamsplitter is mounted on a precision rotator, along with a secondary mirror. Rotation of the beamsplitter allows adjusting the splitting ratio. A set of flat mirrors on precision optical mounts direct the optical beams into two multi-pass cells and direct the cell outputs to focusing optics.

Two multi-pass optical cells provide the needed path length (7.3 m) for a relatively small (and nearly linear) absorption depth of ~10%. These cells are based Aerodyne's 36 m astigmatic Herriott cell, but with the mirrors rotated to the zero-net astigmatism condition, and then with one mirror tipped to allow a full beam pattern. The patterns produced by this cell configuration are well descried by our recent publication on astigmatic cells, given the setup conditions used here [29].

2.4 Temperature and Pressure stabilization and measurement

As we discussed in the preceding section, we have made significant efforts to thermally stabilize the sample and reference multiple pass absorption cells, especially by

enclosing the two cells in a shared thermal zone to minimize and stabilize any temperature gradients. Since the actual gas temperature in each cell is what matters, the sample gas flow is thermally equilibrated with the sample cell before entering the cell (and before the primary pressure drop), by means of ~ 2 meters of copper tubing in thermal contact with the cell enclosure. Since the reference cell flow is so slow, it does not need a copper pre-heating tube.

The temperature of each cell is measured using a high precision thermistor that is either coupled to the cell body in the first version of the instrument or inserted into the gas flow stream in later versions. The temperature readout circuit is based on a high precision voltage source and load resistor, each of which has a small temperature coefficient. These electronics are further stabilized by installing them inside the temperature controlled optics enclosure.

The instrument has both excellent relative temperature stability and excellent temperature measurement capability, as shown by an Allan plot [31, 32] of the temperature ratio between the cells (Figure 4). The short term variance in the temperature ratio of the two cells is 2×10^{-5} in 1 s (equivalent to a precision of 4 mK in each cell). With five minutes of averaging the variance in the measurement falls to 2×10^{-6} or less than 1 mK equivalent precision. Over the entire measurement time (18 hours), we detect no significant change in the ratio of temperatures of the two cells. Thus, we exceed the precision needed to measure at the level of 0.1‰ (i.e. ~8 mK for $^{13}\delta$, ~5 mK for $^{18}\delta$).

Our approach to pressure stabilization is to use a pair of flow controllers installed on the inlets of the two multiple pass absorption cells. Each flow controller is referenced to a pressure sensor and the flow controller is adjusted to maintain a constant pressure. One pressure sensor is an absolute sensor (100 Torr range) that monitors the reference cell (~0.05 liters/minute). The second pressure sensor is a differential sensor (+/- 1 Torr range) connected between the two cells and is used to control the gas flow into the sample cell (1 to 10 liters/minute). The use of one absolute sensor and one differential sensor allows us to balance the pressure in the two cells with greater accuracy. To further improve the stability of the pressure control system, the flow controllers, their drivers and the pressure sensors are all installed within the temperature controlled optics module. In addition, the offset on the differential pressure sensor is automatically measured periodically and accounted for in the flow control system.

Figure 5 shows an Allan plot of 24 hours of pressure measurements obtained using the method just described. We attribute the initial rise in variance to the time constant of the control loop. The pressure control is excellent with a variance at 30 second averaging time of only 1.8×10^{-4}, which corresponds to a differential pressure variance of only 9 mTorr. Furthermore, the actual measured pressures are used in the calculations of the mixing ratios in Eq. 2. We have no evidence of variations in the sample or reference pressure causing significant variations in the retrieved isotopic ratios.

2.5 Dilution Calibration Method

We have described in earlier sections the spectral ratio measurement method and the way that quantitative concentrations result. However, that is only part of the problem in reporting isotopic ratios. For each isotopic ratio we need to combine four measurements into a super ratio (**R**), e.g:

$$^{13}\mathbf{R} = \frac{([366]_{sample} / [266]_{sample})}{([366]_{standard} / [266]_{standard})} \quad . \qquad (3)$$

Thus, to derive an isotopic ratio or delta value ($\delta = \mathbf{R}$-1), one needs to measure four quantities with similar precision. This introduces the classical problem of isotopic instrument calibration. Typically, one will perform a set of measurements, interleaving sample and standard in relatively rapid succession. Ideally, the sample and standard will be at the same concentrations, since instrumental nonlinearity may cause apparent changes of isotopic ratios with concentration. A common calibration approach is to measure the instrument response with a variety of calibration gases with different CO_2 concentrations and isotopic abundances, and then interpolate measured points between this finite set of calibration points.

We have developed a method that simplifies the formation of the isotopic ratios, and which reduces the number of gas standards that are needed. We form a continuous "standard-line" based on the instrument response to dynamically diluting a standard gas with CO_2-free air. The input standard gas has a concentration that varies over the range expected in atmospheric sampling, but with a constant isotopic ratio (assuming that the particular dilution process does not fractionate the isotopologues). Thus one gas tank can serve as many, all with the same isotopic ratios. A period of cyclic dilution produces a measurement of the nonlinear instrument response, which is then fit as a continuous function, the "standard-line" that we use to compare to sample measurements. The tank of standard gas used to generate the standard-line may be at very high concentration, so that after accounting for dilution to ambient levels, the rate of consumption of the standard can be quite low.

To describe the details of the method, we will use the example of one isotopic ratio ($^{13}\delta$), but the same arguments hold for ($^{18}\delta$). We describe the concentrations reported by the instrument as "signals", which are functional approximations of the actual concentrations, i.e.,

$$^{12}S = {}^{12}S([^{12}C^{16}O_2]) \; , \quad ^{13}S = {}^{13}S([^{13}C^{16}O_2]) \quad .$$

No matter how good the spectral measurement we expect that the concentration signals will show some level of zero offsets, non-unity gain-factors, nonlinearities, and possibly cross coupling. When we cycle the concentration of the standard gas (sg), we collect data pairs $^{12}S_{sg}$, $^{13}S_{sg}$, but the actual concentration may not be well known, i.e. only as indicated by $^{12}S_{sg}$. We make a fit function to represent the dynamic dilution, $\mathbf{^{12}\$_{sg}} \approx {}^{12}S_{sg}$. We then collect a set of data points for the sample $\{^{12}S_i \, , \, ^{13}S_i \}$. For the isotopic ratios,

we compare each sample point to the response of the instrument to the standard gas (via the fit function $^{12}\$_{sg}$) at the same concentration [$^{12}C^{16}O_2$] (as indicated by $^{12}S_i$). Suppose we make an approximate isotopic ratio for the sample compared to the standard gas using the concentration signals,

$$\boldsymbol{R'}_{i,\,sg} = \{ (^{13}S_i) / (^{12}S_i) \} / \{ (^{13}\$_{sg}(^{12}S_i)) / (^{12}S_i) \} \quad . \qquad (4)$$

The $^{12}S_i$'s cancel out, leaving only:

$$\boldsymbol{R'}_{i,\,sg} = (^{13}S_i) / (^{13}\$_{sg}(^{12}S_i)) \quad . \qquad (5)$$

If the non-ideal effects in the concentration signals are small, then this simple ratio does a good job of representing the isotopic ratio. In a future paper, we will describe how well this approximation performs with various types of non-ideal effects in the measurement system.

A second standard gas with a different isotopic ratio may be added in a second dynamic dilution cycle, to form a second "standard-line" for comparison. A second standard-line should give improved accuracy, especially when the non-ideal effects in the concentration signals are larger or the isotope ratio of the sample differs strongly from that of the standard gas. In either case, with one or two standard gases, we form a continuous (fit) function to represent the instrument response to the standard gas, and compare to that function at the sample measurement at the same concentration [$^{12}C^{16}O_2$]. To date, we have only done preliminary implementation of the dual standard-line for referencing the data, and most of our data analysis has been with the single standard-line method.

The variable CO_2 dilution flow system uses a cylinder of compressed CO_2 as a secondary isotopic standard and dynamic dilution with CO_2-free air to periodically deliver variable CO_2 mixing ratios to the inlet of the sampling system. A range of mixing ratios from 330 to 500 ppm is used to bracket the range of atmospheric variability encountered at the local measurement site. The CO_2 can be either highly concentrated (1% in N_2) or 100% CO_2. The isotopic composition of this secondary standard must be compared occasionally to a primary standard to monitor any changes in fractionation during expansion from the high pressure cylinder to ambient pressure, although such changes are slow at the low flow rates employed. The flow from the pure CO_2 tank is set to run continuously to avoid any transient fractionation during abrupt pressure changes that could accompany valve switching.

The CO_2-free dilution air is produced with a commercial FTIR purge gas generator (Whatman Model 75-62). Typical conditions with pure CO_2 use a flow of 0.01 lpm diluted with a continuous flow of 0.6 lpm purge gas. A small fraction (10%) of this flow is periodically mixed into a larger variable flow of CO_2-free air. The flow rate is varied from 2 to 3 lpm repeatedly for five 1-minute cycles using a programmed flow controller. This variably diluted flow is switched hourly to over-blow the sample inlet.

CO_2-free air is also added on a separate hourly cycle to account for instrumental zero drift.

The calibration flow is added to the upstream end of the 6 mm od sampling line in order to maintain as close to identical conditions during calibration as during atmospheric sampling. However, the FTIR purge gas generator is dry and the sample air is not dried before the instrument. In our initial experiments, we choose not to dry the ambient air to avoid fractionation or exchange during the drying procedure, which may be particularly relevant for $C^{18}OO$. Further testing is required to decide whether the errors introduced from comparing dry calibration gas to humid sample gas are greater than the errors induced by drying the sample.

3. Results

3.1 Noise and stability

The long term stability of the thermally stabilized prototype dual cell QCL has been evaluated using the Allan variance technique [31, 32], as shown in Figure 6. Figure 6 is based on a 3 hour time series with ambient (lab) air in both cells, and the data analyzed is the simple concentration ratios, [366]/[266], and [286]/[266]. The instrument had a liquid nitrogen cooled HgCdTe detector at the time. The plot shows a 1-sec RMS of 0.1 ‰, and a minimum σ_{Allan} of 0.02 – 0.03‰ after 400 sec integration. Thus, the fundamental precision available is sufficient for useful real-time measurement of these isotopologues of CO_2.

These results are a significant improvement on our previously published results [19], for which we did not use a reference cell, but relied instead on the dual pathlength approach. In those experiments we found a 1-sec rms of 0.5 ‰, and a minimum σ_{Allan} of 0.1‰ at 200 sec. Thus, the most recent results using the dual cell, pulsed QCL approach are approximately 5 times better than our earlier results with the dual pathlength approach.

3.2 Measurement of NIES-characterized samples

We evaluated the linearity and potential accuracy of the instrument prototype by measuring a set of CO_2 samples that were carefully measured with Isotope Ratio Mass Spectroscopy (IRMS) at the National Institute for Environmental Studies (NIES), Tsukuba, Japan. Four carbon dioxide samples were provided with known values of $^{13}\delta$ (-14 to -8 ‰) and $^{18}\delta$ (-8 to 0 ‰). The samples were introduced into our instrument in a programmed cycle, switching between samples every 5 minutes for two hours. In this case we calculated the deltas in relation to reference-lines made with dilution of other CO_2-air mixtures. The raw measurement results for [366] are shown in Figure 7, with four sets of points for the NIES samples and three dilution reference lines (from three different tanks). The plot is made in terms of coordinates (13S'/12S') vs 12S', where the primes indicate that zero-gas responses have been subtracted. This coordinate choice allows us to clearly see the linearity of the reference lines, and their slight slope.

Calculation of isotopic deltas for the samples relative to the dilution reference lines leaves us with the problem of then determining the delta of the dilution reference gas relative to accepted standards. In these measurements we did not have separately characterized standard tanks. Instead, we derive NIES sample deltas relative to those tanks, and then do a linear regression analysis to determine the tank deltas. Our measurement of the samples showed excellent agreement, with correlation slopes between our values and NIES values of 0.95 to 0.97, and residuals from the correlations of 0.02 to 0.03 ‰. Comparing to different reference lines (Tanks Y375 and W403 in Figure 7) produced similar results. A plot of relative-deltas and NIES-listed deltas are shown in Figure 8 using the reference line from tank Y375.

3.3 Long term stability and potential accuracy

We have conducted a long-term sampling experiment with the prototype instrument, analyzing ambient air drawn from the rooftop at Aerodyne Research, Inc from December 2006 through September 2007. The sampling experiment was conducted even as we further developed the instrument system and made changes on the optical table. The data set with the more mature instrument system, from March 2007 onward, will be the subject of an upcoming paper. The matured instrument system was operated in a measurement cycle that included hourly dilution references, plus additions of zero-gas and a fixed concentration gas that acted as a comparison standard.

The long sampling experiment with its periodic additions of a comparison standard provides an opportunity to access the stability and potential accuracy of the instrument. In data from June, 2007, the standard was measured for ~60 seconds every two hours by over blowing the rooftop sampling line to the same conditions, except for humidity, used in the ambient samples. Histograms for the replicate measurements for the month of June are shown in Figure 9. The distributions are nearly Gaussian, with standard deviations 0.19 ‰ for $^{13}\delta$ and 0.29 ‰ for $^{18}\delta$. These results were obtained even though we changed the detectors mid-month. If we separately consider the two weeks before and after the detector change, the distributions of the standard measurements were narrower: $\{\sigma(^{13}\delta), \sigma(^{18}\delta)\} = \{ 0.15, 0.23\}$ for the first two weeks and $\{ 0.11, 0.18 \}$ for the next two weeks. Changing the detectors caused a shift in the average of the replicate measurements of 0.1 ‰ for $^{13}\delta$ and 0.2 ‰ for $^{18}\delta$. Thus the instrument shows excellent stability, even with a change of the detectors.

The noise and stability of the instrument during ambient sampling has been estimated by modeling out the strong dependence of deltas on CO_2 elevations, and then performing Allan variance analysis on the residuals from the model. Fluctuations in $\delta^{13}C$ that are not described by a model (the residuals) may be due to the limitations of the model, and to noise and instability of the instrument. The model residuals represent an upper bound on variance introduced by the instrument. Much of the ambient sampling data is well described by the Keeling model [7, 33], where $^{13}CO_2$ changes are inversely proportional to $[CO_2]$. Data from all of May, 2007 was modeled with Keeling plots in 4 hour segments, and the Allan variance of the residuals are shown in Figure 10. The

variance minimum, at 256 seconds, corresponds to a standard deviation of 0.047 ‰ for $\delta^{13}C$. We conclude that the instrument's basic noise performance during ambient sampling is at least as good as indicated by this Allan variance plot which is also influenced by actual variations in ^{13}C which may not be adequately represented in the simple Keeling plot description for this location..

4. Summary and conclusions

A pulsed QC laser spectrometer has been designed and implemented to measure carbon dioxide isotopologue ratios in ambient air. Both $^{13}C/^{12}C$ and $^{18}O/^{16}O$ ratios can be obtained in a single spectral window near 2310 cm^{-1}. Using a spectral ratio approach we obtain a precision of 0.2 ‰ for a one second measurement of the $^{13}CO_2$ to $^{12}CO_2$ ratio. Signal averaging improves the precision of this measurement to 0.02 ‰. The spectral ratio method improves precision and accuracy by reducing sensitivity to variations in the laser tuning rate, power and line width. Long term accuracy of 0.2 to 0.3 δ is demonstrated with replicate measurements of the same sample over a one month period. The fast time response, long term stability, and continuous unattended operability of this instrument make it suitable for future eddy flux measurements of CO_2 isotopologues.

Acknowledgements

We would like to thank Dr. Hiroshi Suto of the National Institute for Environmental Studies, Tsukuba, Japan for providing us with the calibrated carbon dioxide standards used in this work. We would like thank Professor Scott Saleska for his valuable insights. This work was funded in part by the U.S. Department of Energy under grant No. DE-FG02-04ER83892.

5. References

1. Bowling, D.R., D.D. Baldocci, and R.K. Monson, *Dynamics of isotopic exchange of carbon dioxide in a Tennessee deciduous forest.* Global Biogeochem. Cycles, 1999. **13**: p. 903-922.
2. Kerstel E. in: de Groot, P.A., *Handbook of Stable Isotope Analytical Techniques, pp. 759–787, Chapter 34.* 2004: Elsevier.
3. Flanagan, L.B. and J.R. Ehleringer, *Ecosystem-atmosphere CO2 exchange: interpreting signals of change using stable isotope ratios.* Trends in Ecology and Evolution, 1998. **13**(1): p. 10-14.
4. Yakir, D. and L.S.L. Sternberg, *The use of stable isotopes to study ecosystem gas exchange.* Oecologia, 2000. **123**(3): p. 297-311.
5. Bowling, D.R., P.P. Tans, and R.K. Monson, *Partitioning net ecosystem carbon exchange with isotopic fluxes of CO_2.* Global Change Biology, 2001. **7**: p. 127-145.
6. Flanagan, L.B., J.R. Brooks, and J.R. Ehleringer, *Photosynthesis and carbon isotope discrimination in boreal forest ecosystems: A comparison of functional characteristics in plants from three mature forest types.* J. Geophys. Res, 1997. **102**: p. 28,861-28,869.
7. Keeling, C.D., *The concentration and isotopic abundances of atmospheric carbon dioxide in rural areas* Geochim Cosmochim Acta, 1958. **13**: p. 322– 334.
8. Keeling, C.D., W.G. Mook, and P.P. Tans, *Recent trends in the $^{13}C/^{12}C$ ratio of atmospheric carbon dioxide.* Nature, 1979. **277**: p. 121-123.
9. Kerstel, E. and L. Gianfrani, *Selected papers of the 1st InternationalWorkshop on "Stable Isotope Ratio Infrared Spectrometry: New Developments and Applications" (SIRIS), September 6–8, 2004, Vienna, Austria.* Isotopes in Environmental and Health Studies, 2005. **41**(4): p. 289 - 291.
10. Yakir, D. and X.F. Wang, *Fluxes of CO_2 and water between terrestrial vegetation and the atmosphere estimated from isotope measurements.* Nature, 1996. **380**: p. 515-517.
11. Saleska, S.R., et al., *Feasibility of $^{13}CO_2$ eddy covariance flux measurements using a pulsed quantum cascade laser absorption spectrometer.* Isotopes in Environmental and Health Studies, 2006. **42**(2): p. 115-133.
12. Ehleringer, J.R. and C.S. Cook, *Carbon and oxygen isotope ratios of ecosystem respiration along an Oregon conifer transect: preliminary observations based on small-flask sampling.* Tree Physiol, 1998. **18**(8_9): p. 513-519.
13. Ferretti, D.F., et al., *A new gas chromatograph-isotope ratio mass spectrometry technique for high-precision, N 2 O-free analysis of delta 13 C and delta 18 O in atmospheric CO 2 from small air samples.* Journal of Geophysical Research, 2000. **105**(D5): p. 6709-6718.
14. Trolier, M., et al., *Monitoring the isotopic composition of atmospheric CO 2: Measurements from the NOAA Global Air Sampling Network.* Journal of Geophysical Research, 1996. **101**(D20): p. 25897-25916.
15. Becker, J., T. Sauke, and M.A.X. Loewenstein, *Stable isotope analysis using tunable diode laser spectroscopy.* Applied Optics, 1992. **31**(12): p. 1921-1927.
16. Bowling, D.R., et al., *Tunable diode laser absorption spectroscopy for stable isotope studies of ecosystem–atmosphere CO2 exchange.* Agricultural and Forest Meteorology, 2003. **118**: p. 1-19.
17. Castrillo, A., et al., *Diode laser absorption spectrometry for 13 CO 2/12 CO 2 isotope ratio analysis: Investigation on precision and accuracy levels.* Applied Physics B: Lasers and Optics, 2005. **81**(6): p. 863-869.
18. Gagliardi, G., et al., *High-precision determination of the 13CO2/12CO2 isotope ratio using a portable 2.008-µm diode-laser spectrometer.* Applied Physics B: Lasers and Optics, 2003. **77**(1): p. 119-124.
19. McManus, J.B., et al., *A high precision pulsed quantum cascade laser spectrometer for measurements of stable isotopes of carbon dioxide.* J. Modern Optics, 2005. **52**: p. 2309-2321.
20. McManus, J.B., et al., *Infrared laser spectrometer with balanced absorption for measurements of isotopic ratios of carbon gases,.* Spectrochim. Acta A, 2002. **58**: p. 2465-2479.
21. Tuzson, B., et al., *Quantum cascade laser based spectrometer for in situ stable carbon dioxide isotope measurements* Infrared Physics & Technology, 2007, doi:10.1016/j.infrared.2007.05.006.
22. Weidmann, D., et al., *Development of a compact quantum cascade laser spectrometer for field measurements of CO 2 isotopes.* Applied Physics B: Lasers and Optics, 2005. **80**(2): p. 255-260.
23. Mohn, J., et al., *High-precision delta 13 CO2 analysis by FTIR spectroscopy using a novel calibration strategy.* Journal of Molecular Structure, 2007. **834**: p. 95-101.
24. McManus, J.B., et al., *Comparison of cw and pulsed operation with a TE-cooled quantum cascade infrared laser for detection of nitric oxide at 1900 cm^{-1}.* Applied Physics B, 2006. **85**(2-3): p. 235 - 241.
25. Nelson, D.D., Jr., et al., *Characterization of a near-room-termperature, continuous-wave quantum cascade laser for long-term, unattended monitoring of nitric oxide in the atmosphere.* Opt. Lett., 2006. **31**: p. 2012-2014.
26. Rothman, L.S., et al., *The HITRAN 2004 molecular spectroscopic database.* Journal of Quantitative Spectroscopy and Radiative Transfer, 2005. **96**(2): p. 139-204.
27. Nelson, D.D., et al., *High precision measurements of atmospheric nitrous oxide and methane using thermoelectrically cooled mid-infrared quantum cascade lasers and detectors.* Spectrochimica Acta A, 2004. **60**: p. 3325-3335.
28. Nelson, D.D., et al., *Sub-part-per-billion detection of nitric oxide in air using a thermoelectrically cooled mid-infrared quantum cascade laser spectrometer.* Applied Physics B, 2002. **75**: p. 343-350.
29. McManus, B., *Paraxial Matrix Description of Astigmatic and Cylindrical Mirror Resonators with Twisted Axes for Laser Spectroscopy.* App. Optics, 2007. **46**: p. 472-482.
30. McManus, J.B., P.L. Kebabian, and M.S. Zahniser, *Astigmatic mirror multiple pass absorption cells for long pathlength spectroscopy.* Applied Optics, 1995. **34**: p. 3336-3348.
31. Allan, D.W., *Statistics of atomic frequency standards.* Proc. IEEE, 1966. **54**(2): p. 221-230.
32. Werle, P., R. Mucke, and F. Slemr, *The limits of signal averaging in atmospheric trace-gas monitoring by tunable diode-laser absorption-spectroscopy (TDLAS).* Appl. Optics B, 1993. **57**: p. 131-139.
33. Pataki, D.E., et al., *The application and interpretation of Keeling plots in terrestrial carbon cycle research.* Global Biogeochemical Cycles, 2003. **17**(1): p. 1022.

Figure Captions

Figure 1. A typical isotopologue-specific spectral scan in the 2310 cm^{-1} region using the dual-cell QCL spectrometer. Data are plotted in green and the real time fit to the data is in blue. The peak absorbance for each species is approximately 10%. The acquisition time was 1 second, the cell pressure 60 Torr and the pathlength 7 meters.

Figure 2. Normalized spectrum. Residual absorbance is negative and small.

Figure 3. Solid model of optical module.

Fig 4. Allan plot of temperature ratio between sample and reference cells. Temperature measurements are reported at 1 Hz. Total data set covers nearly 18 hours.

Fig 5. Allan plot of pressure ratio between sample and reference cells. Pressure measurements are reported at 1 Hz. Total data set covers more than 24 hours.

Figure 6. Allan plots for the concentration ratios [366]/[266], and [286]/[266] measured with ambient (lab) air in both cells. The plot shows a 1-sec RMS of 0.1 ‰, and a minimum σ_{Allan} of 0.02 – 0.03‰ after 400 sec integration.

Figure 7. Plot of ($^{13}S'/^{12}S'$) vs $^{12}S'$ (see text for explanation of S') for three dilution gases (shown as orange, green and blue points) and for the four isotopic standards provided by NIES (shown as blue points). The fit to each dilution curve is displayed as a solid line with the corresponding color.

Figure 8. Plot of relative-deltas determined in this work using infrared spectroscopy with the dilution method versus the NIES-listed deltas determined by Isotope Ratio Mass Spectrometry.

Figure 9. Histograms of replicate measurement of isotopic deltas for a gas standard, measured every two hours during June.

Figure 10: Alan variance analysis on the residual from modeling May 2007 data as a set of Keeling plots, performed on 4 hour segments of data.

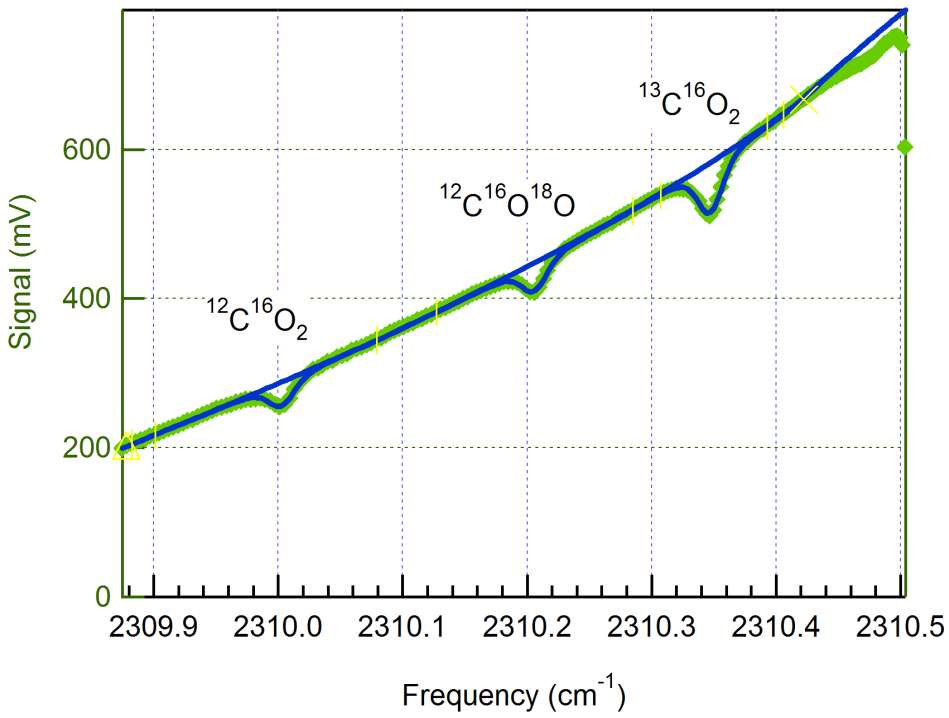
Signal (mV)
0
200
400
600
2309.9
2310.0
2310.1
2310.2
2310.3
2310.4
2310.5
Frequency (cm-1)
12C16O2
12C16O18O
13C16O2

Figure 1.

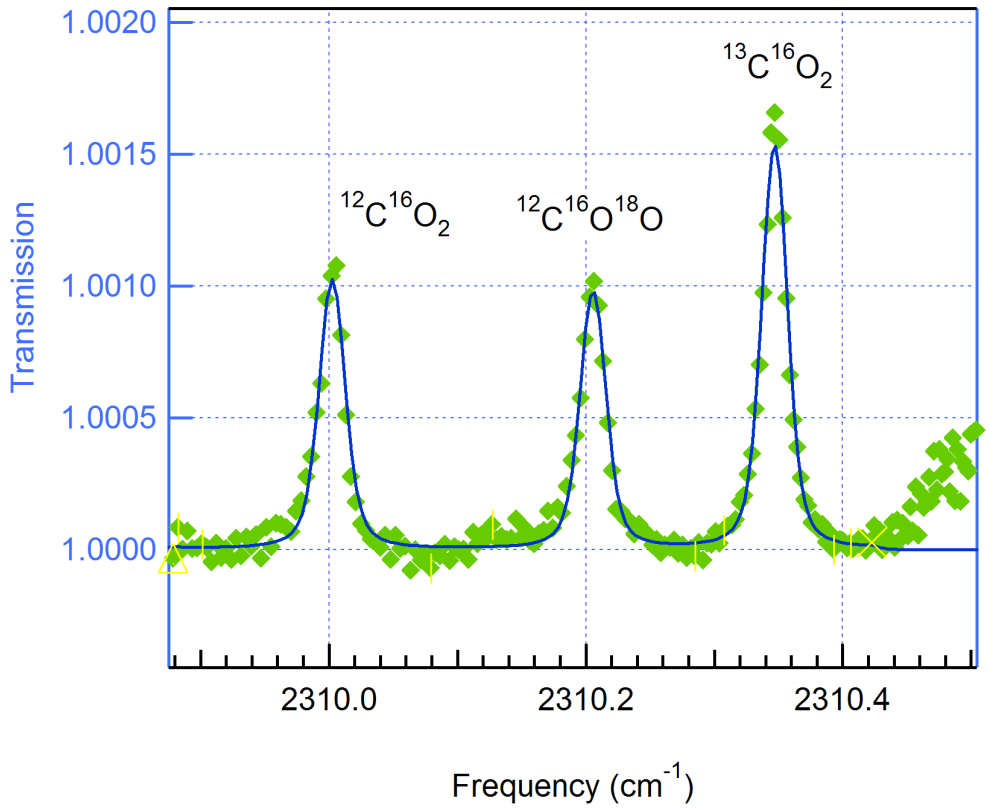
1.0020
1.0015
1.0010
1.0005
1.0000
Transmission
$^{12}C^{16}O_2$
$^{12}C^{16}O^{18}O$
$^{13}C^{16}O_2$
2310.0
2310.2
2310.4
Frequency (cm^{-1})

Figure 2.

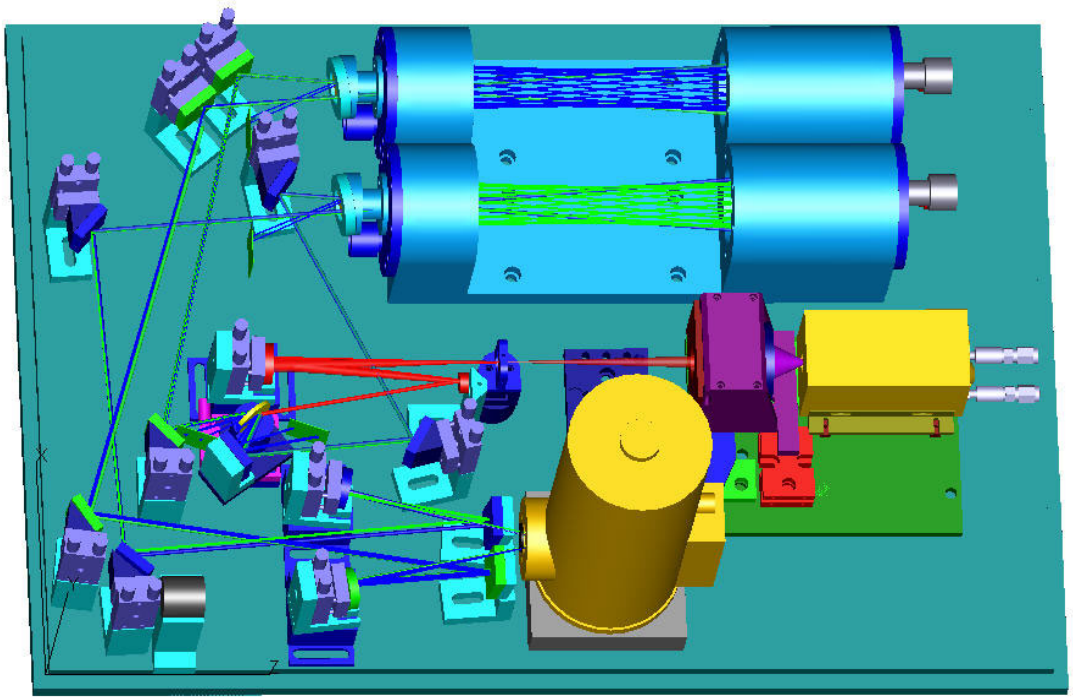

Figure 3.

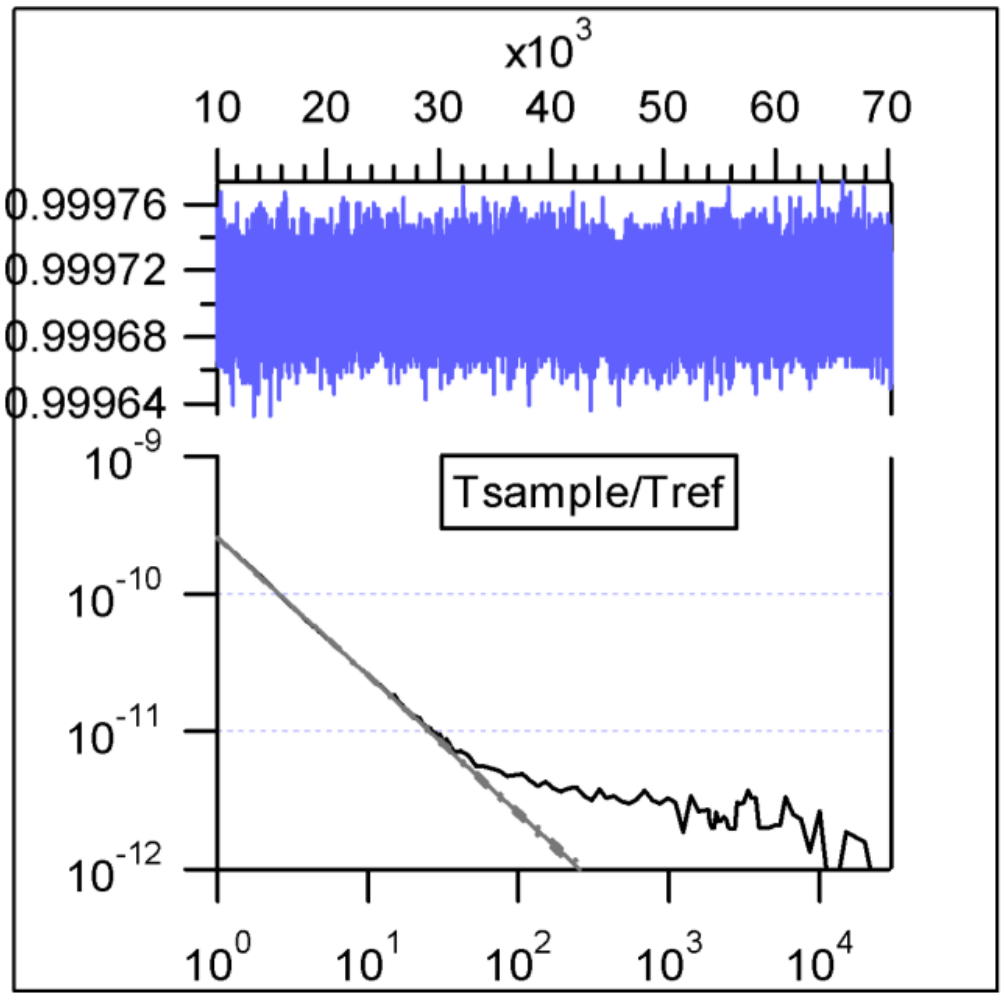
x10^3
10
20
30
40
50
60
70
0.99976
0.99972
0.99968
0.99964
10^-9
Tsample/Tref
10^-10
10^-11
10^-12
10^0
10^1
10^2
10^3
10^4

Figure 4.

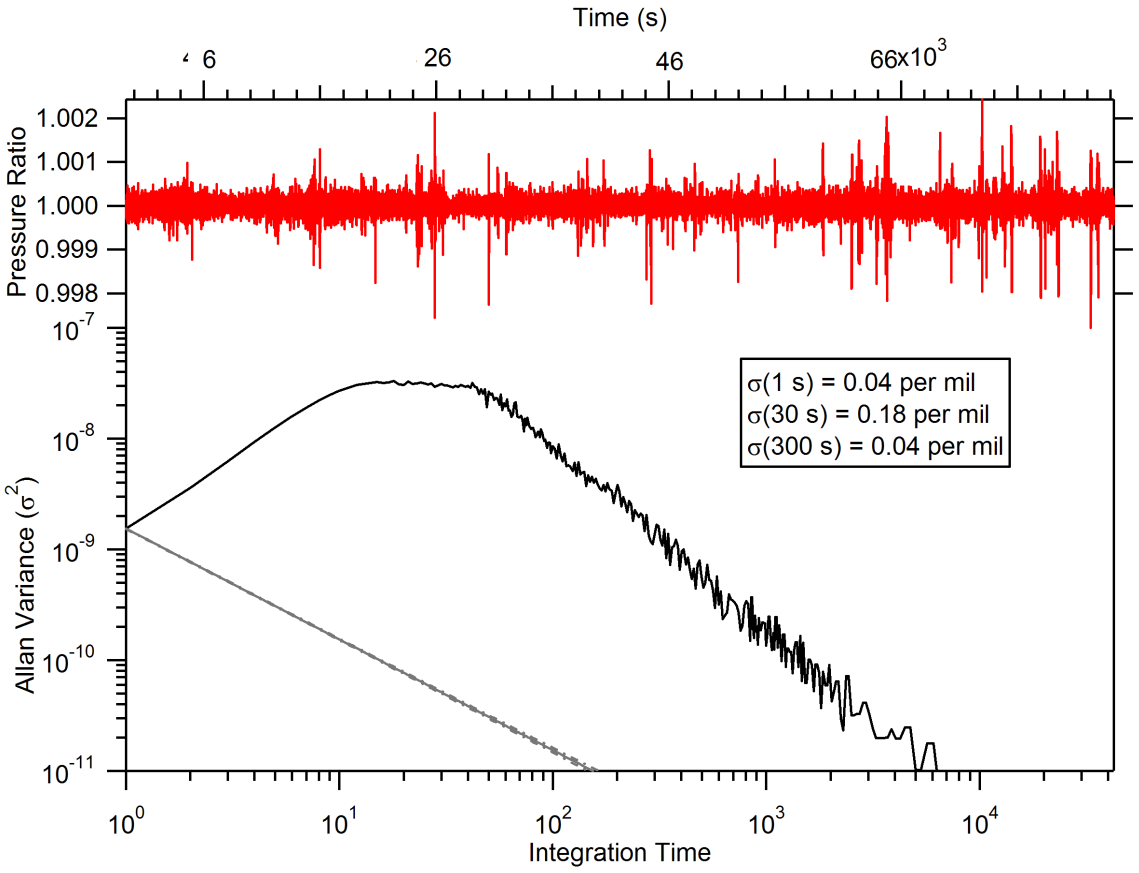
Time (s)
6
26
46
66x10^3
Pressure Ratio
1.002
1.001
1.000
0.999
0.998
10^-7
10^-8
10^-9
10^-10
10^-11
Allan Variance (σ^2)
σ(1 s) = 0.04 per mil
σ(30 s) = 0.18 per mil
σ(300 s) = 0.04 per mil
10^0
10^1
10^2
10^3
10^4
Integration Time

Figure 5.

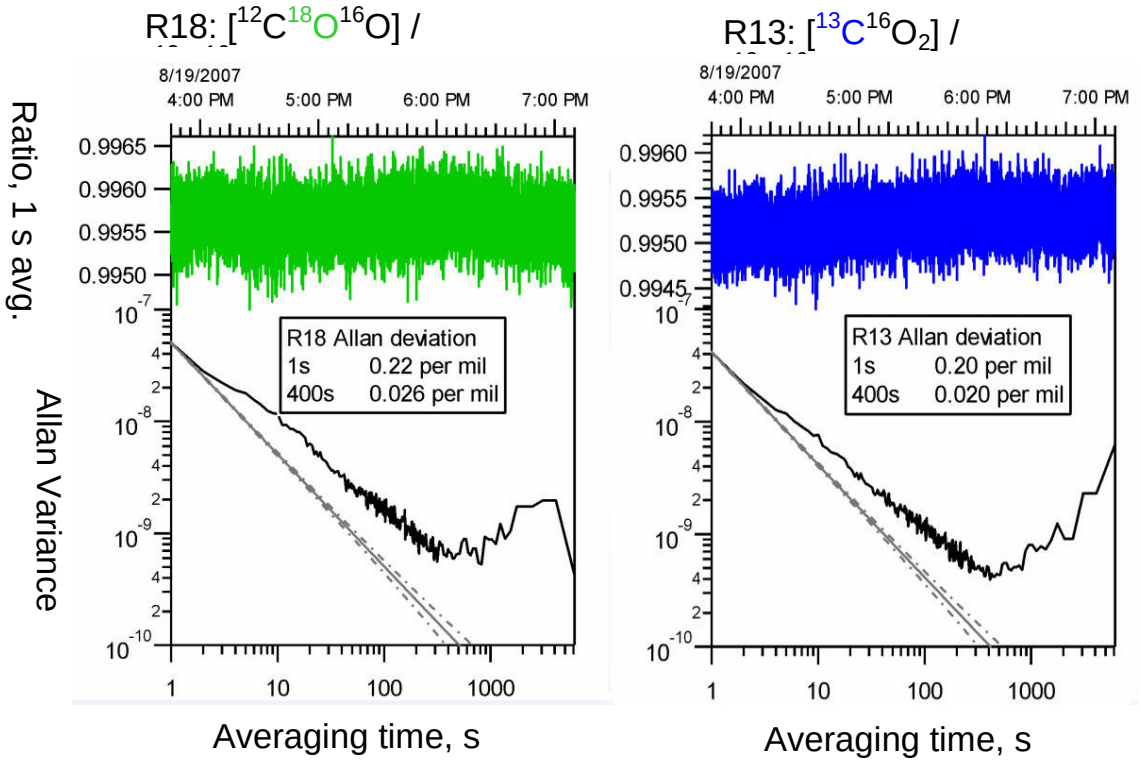
R18: [12C18O16O] /
R13: [13C16O2] /
8/19/2007
4:00 PM
5:00 PM
6:00 PM
7:00 PM
Ratio, 1 s avg.
Allan Variance
R18 Allan deviation
1s 0.22 per mil
400s 0.026 per mil
R13 Allan deviation
1s 0.20 per mil
400s 0.020 per mil
Averaging time, s
Averaging time, s

Figure 6.

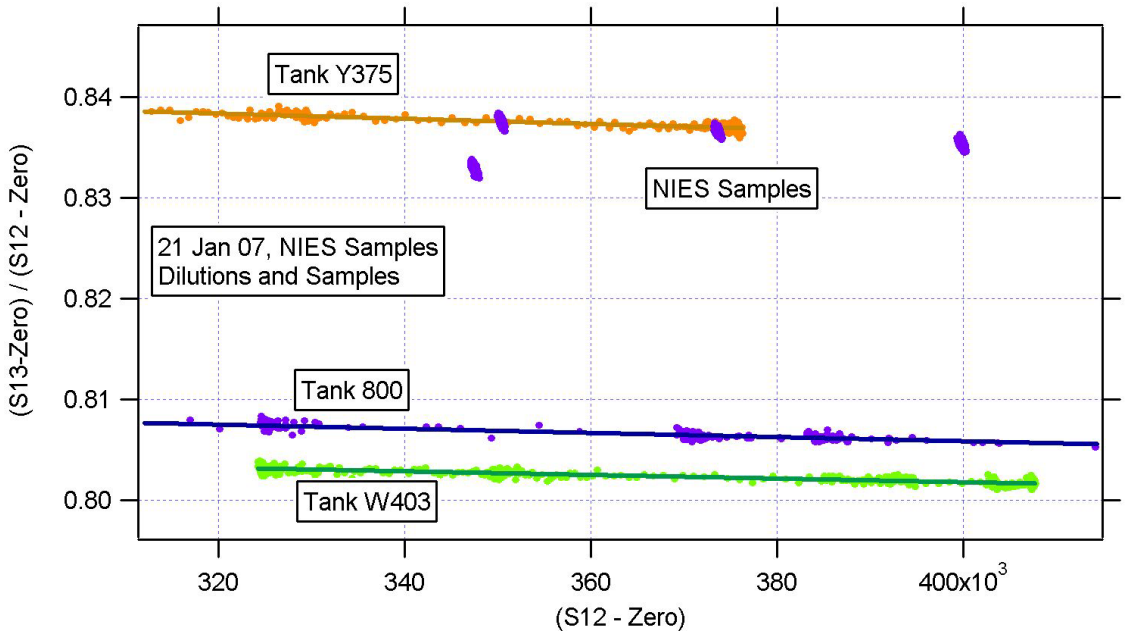
Tank Y375
NIES Samples
21 Jan 07, NIES Samples
Dilutions and Samples
Tank 800
Tank W403
0.84
0.83
0.82
0.81
0.80
(S13-Zero) / (S12 - Zero)
320
340
360
380
400x10^3
(S12 - Zero)

Figure 7.

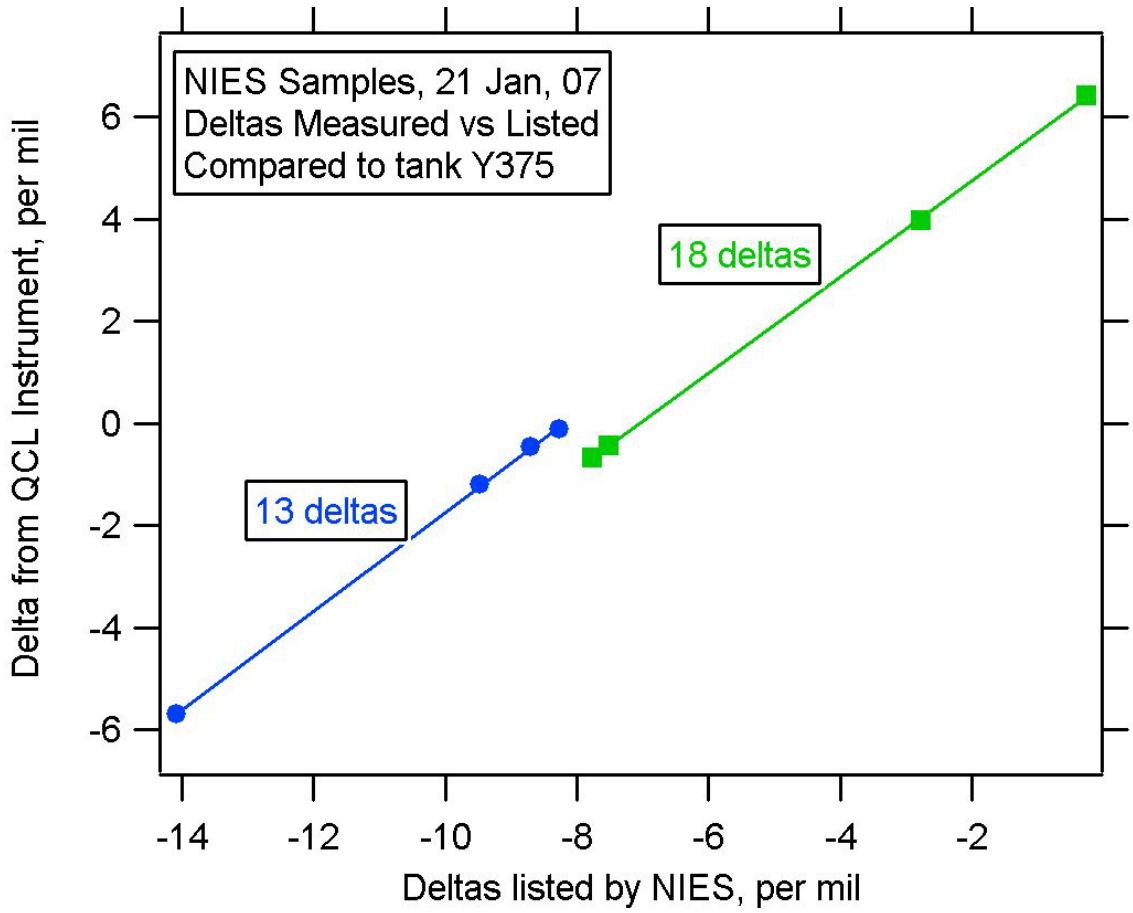
NIES Samples, 21 Jan, 07
Deltas Measured vs Listed
Compared to tank Y375
18 deltas
13 deltas
Delta from QCL Instrument, per mil
Deltas listed by NIES, per mil
6
4
2
0
-2
-4
-6
-14
-12
-10
-8
-6
-4
-2

Figure 8

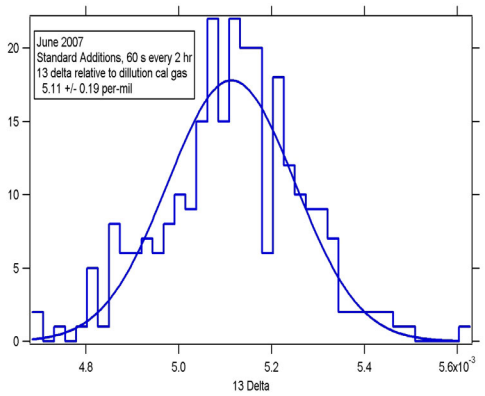
June 2007
Standard Additions, 60 s every 2 hr
13 delta relative to dillution cal gas
5.11 +/- 0.19 per-mil
20
15
10
5
0
4.8
5.0
5.2
5.4
5.6x10-3
13 Delta

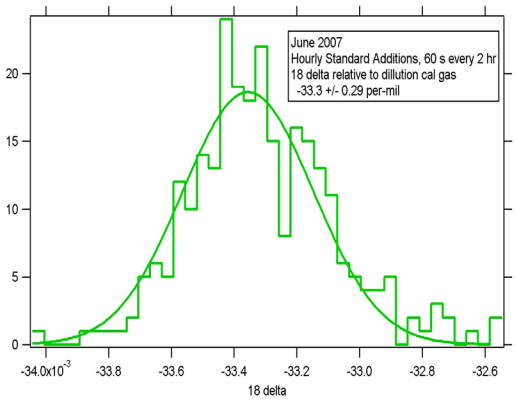
June 2007
Hourly Standard Additions, 60 s every 2 hr
18 delta relative to dillution cal gas
-33.3 +/- 0.29 per-mil
20
15
10
5
0
-34.0x10-3
-33.8
-33.6
-33.4
-33.2
-33.0
-32.8
-32.6
18 delta

Figure 9.

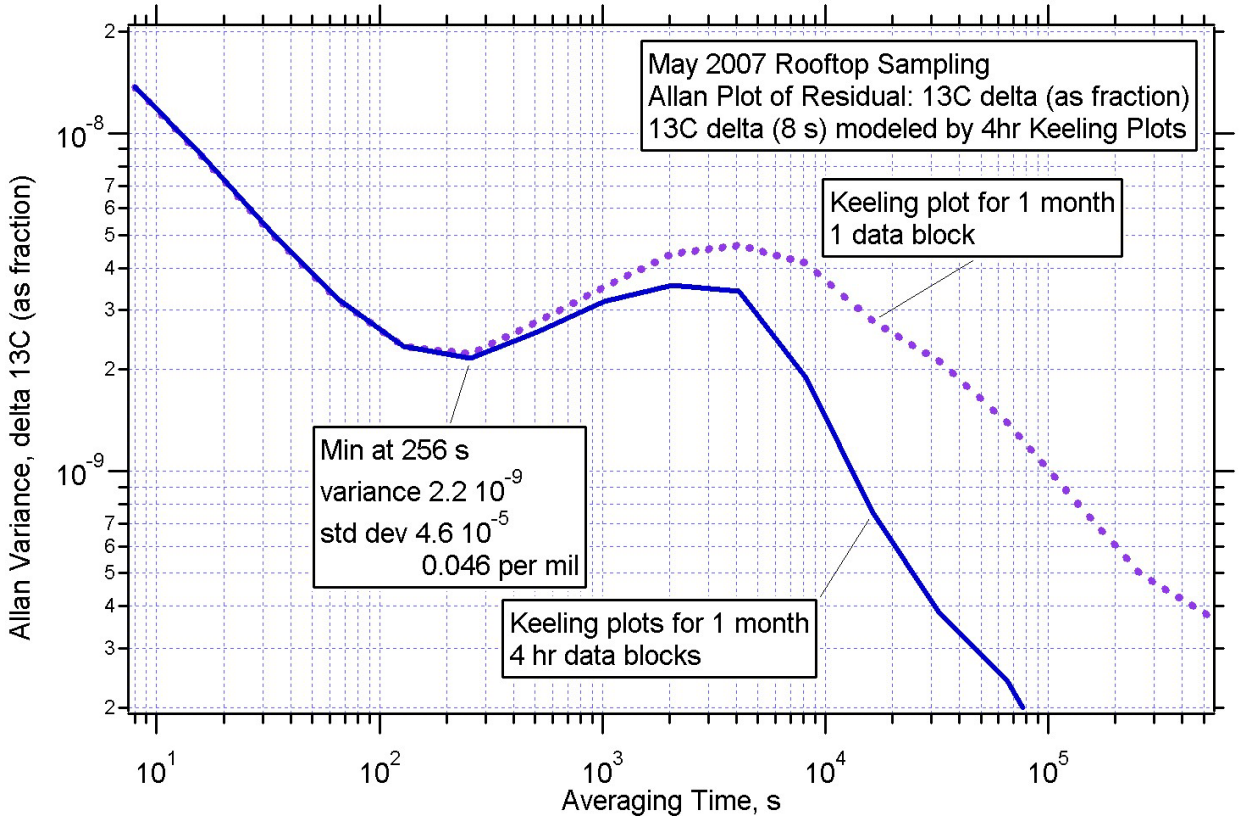
May 2007 Rooftop Sampling
Allan Plot of Residual: 13C delta (as fraction)
13C delta (8 s) modeled by 4hr Keeling Plots
Keeling plot for 1 month
1 data block
Min at 256 s
variance 2.2 10-9
std dev 4.6 10-5
0.046 per mil
Keeling plots for 1 month
4 hr data blocks
Allan Variance, delta 13C (as fraction)
Averaging Time, s

Figure 10.